Co-published by
Institute of Fluid-Flow Machinery
Polish Academy of Sciences
Committee on Thermodynamics and Combustion
Polish Academy of Sciences

http://www.imp.gda.pl/archives-of-thermodynamics/

Parametric Analysis of Heat Transfer and Flow Characteristics of the Cross-Flow Heat Exchanger with a Backwards Splitter Plate Using the Computational Fluid Dynamics (CFD) Model

Sachin Kaushik[a], Subash Chandra Ram[b*], Chandra Kishor[a], Sunii Chamoli[c]

[a]Department of Mechanical Engineering, Graphic Era University, Dehradun 248002, Uttarakhand, India
[b]Department of Mechanical Engineering, Tula's Institute, Dehradun 248011, Uttarakhand, India
[c]Department of Mechanical Engineering, GBPIET, Pauri, Garhwal 246194, Uttarakhand, India
*Corresponding author email: subh.mtech07@yahoo.com

Received: 08.07.2025; revised: 26.01.2026; accepted: 30.01.2026

Abstract

This article investigates the parametric effects on heat transfer in cross-flow heat exchangers integrated with a backward splitter plate to enhance the coefficient of performance in a solar assisted vapour absorption refrigeration system. The system replaces conventional electric energy with solar energy, utilising a solar energy collector to heat water between 50 − 80°C. This heated water vaporises aqueous ammonia in a generator designed as a double pipe heat exchanger. The primary objective is to facilitate efficient heat transfer from the solar energy collector to the solar assisted vapour absorption refrigeration system and evaluate the cooling performance at varying water mass flow rates. Computational fluid dynamics has been used to solve the governing equations under appropriate boundary conditions. While second-order discretisation has been used for momentum and energy equations, coupled equations have been used to address velocity and pressure coupling. Convergence criteria of 10^{-6} for velocity and continuity, and 10^{-8} for energy, were employed. Thermal modelling was conducted to find out component-specific heat transfer rates and estimate the cumulative coefficient of performance. A small-capacity (1.5 ton or 5.25 kW) solar vapour absorption cooling system was tested. The study found that increasing the L/D ratio enhances heat transfer; for instance, at Re = 12000 and L/D = 2, the Nusselt number increased by 90% compared to Re = 2000. However, the pressure dropped significantly at L/D = 3, suggesting an optimal design trade-off. Additionally, the impact of key parameters such as absorber, condenser, generator and evaporator temperatures on the system's coefficient of performance was thoroughly analysed.

Keywords: Parametric analysis; Cross flow heat exchanger; Heat transfer; Back splitter plate

Vol. 47(2026), No. 1, 161–176; doi: 10.24425/ather.2026.158667

Cite this manuscript as: Kaushik, S., Ram, S.C., Kishor, C., & Chamoli, S. (2026). Parametric Analysis of Heat Transfer and Flow Characteristics of the Cross-Flow Heat Exchanger with a Backwards Splitter Plate Using the Computational Fluid Dynamics (CFD) Model. *Archives of Thermodynamics*, 47(1), 161−176.

1. Introduction

The application of the solar vapour absorption technique remains the most feasible choice, given the rapidly changing global energy landscape and the increasing focus on environmental preservation and energy conservation. Solar vapour absorption cooling is a solution to the growing expense of electricity, the worsening power situation, and the increasing emissions of chlorofluorocarbons (CFCs) pollutants. Non-traditional energy sources, including hydropower, geothermal, wind and solar are crucial for mitigating biodiversity loss for a broad spectrum of reasons. When operating, unconventional energy sources emit little or no greenhouse gases (GHGs). The practical application of solar energy has grown significantly over the past few years among unconventional energy sources. In areas that have consistently high levels of sunshine throughout the year, solar

Nomenclature

h – enthalpy, kJ/kg
L/D – length of splitter plate to diameter of tube ratio
$L\times W\times H$– length × width × height (geometrical dimensions)
$\dot{m}$ – mass flow rate, kg/s
Nu – Nusselt number
P – pressure
Pr – Prandtl number
Q_a – total heat transfer rate, kW
Q_{HX} – heat exchanger heat transfer rate, kW
Re – Reynolds number
SD/D – diagonal spacing
SL/D – longitudinal spacing
ST/D – transverse spacing
T – temperature, K
$T_{a,o}$ – outlet air temperature
$T_{a,i}$ – inlet air temperature

Greek symbols

α – inclination angle of splitter plate, °
λ – circulation ratio
ξ – concentration

Abbreviations and Acronyms

CFCs– chlorofluorocarbons
CFD – computational fluid dynamics
CHPC– combined heat, power and cooling
COP – coefficient of performance
GHGs– greenhouse gases
H_2O – water
LHTES– latent heat thermal energy storage
LiBr – lithium bromide
SAVAR– solar assisted vapour absorption refrigeration
SEC – solar energy collector

energy has become a necessity and a daily need. Solar energy consumption is particularly important in these places due to the regularity and amount of sunlight [1−5].

A type of cooling agent is used in the vapour absorption cycle to both absorb and release heat during the condensation and evaporation processes. This process often requires heat, which can be obtained from a variety of fuels or eco-friendly sources like solar energy. A solar-powered vapour absorption refrigeration unit employs solar thermal collectors to provide the heat required to power the absorption cycle, making it more environmentally friendly and energy-efficient than conventional electrically-driven refrigeration systems. Fan et al. [6] claim that an absorption cycle is comparable to a vapour compression cycle, and is predicated on the evaporation or absorption effects that occur when a substance's liquid and gaseous phases interact, each of which has a different vapour pressure. Heat loss to the surroundings is a serious issue with the hot water storage tank. The actual heat loss coefficient, as reported by Jacobsen [7], was 1.65 W/(m^2·K), over 50% higher than the expected value of 1.19 W/(m^2·K). Sometimes, the heat loss through the boiling water storage tank is equivalent to two hours of daily operation of the solar air conditioner. Developing the construction of the lithium bromide solution (LiBr-H_2O) absorption refrigerator with a nominal capacity of 1 kW was considered by Kalogiro and Florides [8]. Absorption refrigerators are machines without moving parts that generate cooling through the use of heat energy.

One of the earliest innovations of the refrigeration system, which is now the most important use of solar energy for cooling, was the vapour absorption cycle. Furthermore, researchers are becoming increasingly interested in the ongoing development of absorption refrigeration systems due to the need for high-grade energy to operate mechanical vapour compression refrigeration systems. Experiments with high LiBr concentrations, extremely close to the solution's crystallisation limit, have been carried out by Charters and Chen [9]. It was observed that crystals would form and the system would "shut down" if the generator's temperature dropped suddenly. It was proposed that to solve this issue; the LiBr-H_2O solution must contain certain salts (such as LiSCN) in order to reduce the solution's vapour pressure and enhance the solution's properties for usage in an air-cooled system. The absorption refrigeration system is more appealing to researchers because it can generate a cooling effect using low-grade energy. Systems based on vapour compression are currently the most widely used air conditioning and refrigeration systems. Because of their proven technology, dependability and affordability, these systems are frequently used. However, in order to function, these systems need high-grade energy, either electrical or mechanical. In addition, scientists have been compelled to explore alternative cooling systems as it was recently discovered that the traditional working fluids of vapour compression systems are contributing to ozone layer depletion and greenhouse effects. The absorption system, which operates mostly on thermal energy, is the obvious substitute. Additionally, these systems operating fluids are environmentally improved.

Choosing the right working fluid is arguably the most crucial component of any refrigeration system. The cycle efficiency and performance characteristics of the absorption refrigeration system are determined by the properties of the absorbent, refrigerant and their combinations. Additionally, absorbent and refrigerant vapour pressure, solvent solubility, solution heat capacity, heat of vaporisation, heat of solution and solution viscosity all affect cycle efficiency. The two most important thermo-physical properties of the solution are its surface tension and thermal conductivity. In addition, toxicity, chemical stability and corrosivity are further selection factors for the working fluids. The energy efficiency of systems like cogeneration or combined heat, power and cooling (CHPC) is increased with the use of absorption chillers. Because absorption chillers have nearly zero running costs when waste heat energy is the source, they are widely used in industries such as textiles, synthetic fibre, chemicals, pharmaceuticals, electronics, beverage cooling, brewing, tobacco and more.

Using the first as well as the second laws of thermodynamics, Mansoori and Patel [10] have established upper and lower constraints for the coefficient of performance (COP) of absorbent cooling cycles. It is shown that these upper and lower limitations are dependent not only on the ambient temperatures of

the cycle's component sections but also on the thermodynamic properties of refrigerants, absorbents and their mixtures. A quantitative comparison of various refrigerant-absorbent combinations can be conducted using these upper and lower bounds of COP. The H_2O-NH_3, NH_3-NaSCN and LiBr-H_2O combinations, all of which are viable choices for solar absorption cooling cycles, are compared using the developed approach. Vapour absorption refrigeration/cooling systems belong to the same class of vapour cycles as vapour compression refrigeration systems. However, absorption systems require heat as an input, in contrast to vapour compression refrigeration systems. As a result, these systems are often known as thermal energy-driven or heat-operated systems. Both vapour compression and absorption refrigeration cycles remove heat by allowing a refrigerant to evaporate at low pressure and reject heat by allowing the refrigerant to condense at a higher pressure. The main difference is that a vapour compression technology uses a mechanical compressor, whereas an absorption method uses a heat source to create the pressure differences needed to circulate the refrigerant. Because of these distinctions, an absorption system needs little to no work input, but heat must be supplied as energy. The system becomes more attractive when there is a low-cost heat source, such as solar heat or waste heat from power or heat generation.

Zhang et al. [11] conducted a comprehensive review of previous studies on the use of heat transfer enhancement strategies in plate heat exchangers, with a focus on passive surface methods and the use of nanofluids. The study showed that the thermal-hydraulic capabilities of the investigations employing different parameters of geometry and augmentation procedures are frequently higher for relatively small Reynolds numbers. Similarly, Awad and Muzychka [12] analysed and investigated the thermal-hydrodynamic characteristics of air-cooled tiny wavy fin heat exchangers. They released new models that facilitate the prediction of the Fanning and Colburn friction factors. To enhance the system's functionality, since energy losses are the cause of system performance decline, the irreversible nature should be assessed during the cycle. The COP is commonly used to assess a vapour compression system's effectiveness.

COP does not reveal the system component elements' thermodynamic equilibrium deterioration. The losses of energy in vapour compression refrigeration systems can be measured with the use of exergy evaluation. As the temperature differential between the system and its surroundings increases, so do the energy losses [13]. Ghamati et al. [14] investigated the flow patterns and energy transmission of natural convection using nanofluid technology in enclosed areas that are square, circular and hexagonal in shape. The study's findings demonstrated that the final equations were validated through prior research and solved numerically. For a variable that stays constant in the temperature index (n), the results showed that increasing the Prandtl number (Pr) from about 0.1 to 2 reduces the skin friction coefficient by approximately 32% and the velocity at its maximum by slightly more than a half. Because the temperature that is dimensionless drops to zero faster in this case, the thermal boundary layer thickness falls, and the Nusselt number (Nu) rises. The effective COP for heat exchangers with a finned backward splitter plate was shown to be lower for solar-assisted vapour absorption refrigeration (SAVAR) systems, which is an intriguing area of scientific study.

Beyond the general literature, several focused studies have explored performance improvements in LiBr–water absorption cooling systems. One such study examined the use of a plate heat exchanger as a pre-cooler for the absorber, showing that this setup could reduce absorber size by 6–14%. Notably, channelling just 20% of the total cooling water flow through the pre-cooler was enough to yield significant efficiency gains [15]. Another study developed a simulation model of a solar-powered LiBr–water absorption system with auxiliary heating, analysing the effects of changes in the atmospheric clearness index. A decrease in the index from 0.63 to 0.52 resulted in a 67% increase in the auxiliary heat requirement to maintain consistent cooling performance [16]. In recent years, both experimental and theoretical work has advanced in the field of solar-assisted absorption and adsorption refrigeration (AR) systems. For example, Sumathy and Li [17] experimentally investigated a solar-driven adsorption system using an activated carbon–methanol pair. Their setup, which utilised a flat plate solar collector with an exposed surface area of 0.92 m^2, achieved a COP between 0.10 and 0.12. Similarly, Pons and Guilleminot [18] conducted experiments on a solar-powered adsorption chiller using the same activated carbon–methanol working pair, achieving a COP of approximately 0.12. Dawoud [19] developed a hybrid solar-assisted adsorption cooling system tailored for vaccine storage applications. In another study, Ghali et al. [20] evaluated the hourly performance of a hybrid cooling system incorporating a desiccant wheel for air conditioning in a typical auditorium. Their work included a comparative analysis with conventional air conditioning systems under the climatic conditions of Beirut. The system included a 1.5 m^3 thermal storage tank, a vacuum flat-plate solar collector with a total aperture area of approximately 42.2 m^2 and a 25 kW plate heat exchanger. Additionally, Abu Ein et al. [21] conducted a thermodynamic assessment of a 10 kW solar-powered ammonia–water absorption chiller, utilising both first and second law analyses to evaluate its performance. Further research has also explored the integration of thermal energy storage in LiBr-H_2O absorption systems to mitigate mismatches between thermal energy supply and cooling demand. Various system configurations have been investigated, focusing on performance metrics such as COP and energy storage density (ESD). Important findings showed that under ideal circumstances, ESD values ranged from roughly 119.6 kWh/m^3 to 444.3 MJ/m^3, and COP values ranged from 0.69 to 0.99 [22]. Low-temperature-driven LiBr–water absorption heat pumps have also been developed with innovative modular designs, namely, "Bee", "Bumblebee" and "Hornet". Operating at driving water temperatures around 90°C, these systems achieved thermal COPs of approximately 0.8 while maintaining a compact form factor. Several commercial models have been deployed in pilot-scale solar cooling applications [23]. In a separate study, a compact cross-flow heat exchanger was assessed as an air heater in a solar tunnel dryer. The device enabled heat transfer between ambient air and hot water supplied by a parabolic trough collector. Findings showed that increasing the air mass

flow rate improved the heat transfer rate but simultaneously decreased the overall effectiveness of the heat exchanger [24]. Additional research explored the impact of solar radiation on the thermal performance of a cross-flow wet cooling tower under hot climate conditions. It was observed that the use of a sunshade led to significant performance improvements, with outlet water temperature, temperature range and thermal efficiency increasing by up to 37% [25]. This study has explored the impact of incorporating a backward splitter plate within a cross-flow heat exchanger on heat transfer characteristics and the overall enhancement of the COP in a SAVAR system. In this configuration, conventional electrical energy has been substituted with solar energy via a solar energy collector (SEC), which heats water within the range of 50 – 80°C. The resulting thermal energy is used to vaporise aqueous ammonia in a double-pipe heat exchanger serving as the generator. The primary aim is to optimise heat transfer and assess the cooling performance of the system across varying water mass flow rates. Additionally, the study presents a comparative evaluation of three refrigerant-absorbent pairs: H_2O-NH_3, NH_3-NaSCN and LiBr-H_2O to determine their suitability for use in solar absorption cooling systems. Unlike conventional vapour compression systems, which depend on mechanical energy input, absorption systems are driven by thermal energy, making them particularly suitable for integration with low-cost energy sources such as solar or industrial waste heat.

Although prior research has examined solar-assisted absorption systems, several critical gaps remain. Notably, the influence of geometric modifications such as the addition of a backward splitter plate on internal flow distribution and thermal performance within heat exchangers has not been comprehensively addressed. Furthermore, the system's performance under dynamic solar radiation conditions and its long-term efficiency across seasonal variations are under-investigated. Finally, while refrigerant absorbent combinations are often assessed based on thermal performance, there is a lack of multi-objective optimisation studies that consider economic feasibility, environmental impact and operational reliability factors essential for the widespread practical adoption of these systems. The system's thermodynamic analysis was carried out to determine which components were subject to heat transfer. The system performance was then calculated, and COP was enhanced. The present experimental research has used a solar energy vapour absorption cooling system with a small capacity (1.5 ton or 5.25 kW). Additionally, the impact of variables affecting the system COP, such as the temperature of the condenser, generator, absorber and evaporator, was examined.

These heat exchangers can be designed and analysed through numerical analysis, experimentation or the use of computational fluid dynamics (CFD) software. The science of CFD uses digital computers to generate quantitative forecasts of fluid-flow phenomena based on the mass, momentum and energy conservation laws that govern fluid motion. The majority of CFD software tools, which were created to aid in the rapid resolution of heat exchangers, can forecast heat distributions and boost flow system efficiency. CFD methods have been used in a number of studies on cross-flow heat exchanger performance. Computational fluid dynamics simulation can also be used to improve the performance of an existing heat exchanger even when it has heat pipes. The CFD simulation was used to examine how altering the pipe diameter and the angle between the pipes could improve performance, which was then applied to the heat exchanger under study. This method's high adaptability and reduced simulation time make it a viable option for other heat exchanger designs that incorporate heat pipes [26,27].

It has been demonstrated that using splitters to manage the separated wake downstream of the pin-fins is beneficial [28]. Ul-Islam et al. [29] investigated the effects of the length of dual splitter plates positioned at the front and rear sides of two adjacent square cylinders on flow characteristics and fluid force reduction. It was found that the splitter plate placed behind the cam-shaped cylinder functions as an appropriate passive control mechanism to successfully limit vortex shedding and lower drag. This device can be used to minimise drag in bluff bodies and cam-shaped cylinders [30]. Tu et al. [31] predicated on the impact of the centre cylinder in a five-cylinder array, which has been illustrated by altering the spacing ratio. Elmekawy et al. [32] investigated on cross-flow staggered tube banks of cylinders with splitter plates attached to the tubes. Their study demonstrated an improvement in thermal performance by providing a more streamlined flow through the splitter plates in the downstream section of the tubes. This design reduces the interactions and intensities of vortices and eddies, as well as energy losses. However, a 16–20% rise in pressure drop was reported [32].

Hishikar et al. [33] investigated that the multi-cylinder arrangement enhances the rate of heat transfer by allowing for vortex shedding and turbulence to occur in the spaces between the cylinders. Another research was on creating a computational fluid dynamics model to describe the heat transfer in a boosted diesel engine cross-flow plate heat exchanger [34]. Pressure distributions, vorticity and pathline structures were used to comprehend the phenomena of heat transfer and flow, while an analysis of drag, lift and the Nusselt number was conducted. Heat transfer by two distinct clusters of nine circular cylinders was analysed using two-dimensional unsteady calculations. The cylinders were exposed to a cross-flow of air in ambient conditions while being kept at constant-heat-flux wall conditions [35]. Heat exchangers, nuclear reactors and electronic circuit boards are just a few examples of engineering devices that display flow separation and reattachment. These device components, which resemble stepped channel designs, are designed to lessen the effects of thermal stress. Another research was reported on the properties of heat transfer and fluid flow using a double backwards-facing step with elliptic obstacles placed after each step. An internal code based on the streamline upwind/Petrov-Galerkin finite element method is used to solve the equations governing fluid flow and heat transfer in a Cartesian framework for this purpose [36].

The performance of heat transfer and the flow structure of a swirling jet on a flat target surface are the main topics of the study. The analysis is performed by varying the number of vanes with Reynolds numbers between 11 200 and 35 600, using helicoid inserts with the swirl number S = 1.3. The performance of swirling and circular jets in terms of heat transfer is compared. According to the heat transfer results, the triple helicoids' axial

recirculation zone at Re = 29 800 and Re = 35 600 has an impact on the uniformity of heat transfer distribution [37]. The flow regime transitions around two adjacent square cylinders under the influence of attached upstream splitters were analysed computationally. The lattice Boltzmann method is employed as a numerical technique for this work. The effect of two influencing factors, the splitters' length (SL) and the cylinder spacing ratio (SR), is highlighted. At a fixed Reynolds number of 150, both parameters are varied between 1 and 4 times the characteristic length (d). In contrast to the situation of two side-by-side cylinders without splitters, the results show an early transition to a synchronised flow regime because of splitters [38].

This study introduces the novel incorporation of a splitter plate within the flow domain of the generator or absorber in a SAVAR system. The geometric modification strategically alters fluid flow patterns, enhancing heat and mass transfer processes critical to the absorption cycle. The presence of the splitter plate promotes more uniform flow distribution and suppresses thermal stratification. This leads to improved heat exchange efficiency between the working fluid and the heat source (solar energy), optimising the energy input required for desorption in the generator. Comparative simulations and experiments demonstrate that the inclusion of the splitter plate results in a noticeable increase in COP of the SAVAR system. This improvement is attributed to better thermal energy utilisation and reduced irreversibilities in the absorption-desorption cycle. Unlike conventional enhancement techniques that require additional mechanical or control systems, the splitter plate serves as a passive method to control flow dynamics, offering a cost-effective and energy-efficient design enhancement. By boosting the performance of solar-assisted vapour absorption systems, this work contributes toward more sustainable and energy-efficient refrigeration technologies, aligning with the global goals of reducing reliance on fossil fuels and minimising environmental impact.

2. Experimental procedure

In this study, CFD simulations and the renormalisation group (RNG) k–ε turbulence model have been employed. This model was chosen due to its enhanced accuracy and reliability in capturing the effects of turbulence in recirculating and swirling flows, which are common in heat exchanger and thermal system applications, particularly in SAVAR systems. The renormalisation group (RNG) k–ε model offers several advantages over the standard k–ε model:

- It incorporates an additional term in the ε equation to account for the interaction between turbulence dissipation and mean shear, which improves performance in rapidly strained and curved flows.
- It provides better predictions for low Reynolds number and near-wall flows compared to the standard model.
- It is computationally more efficient than more complex models like k–ω SST, making it suitable for simulations involving large domains or long transient runs.

2.1. Design of the solar assisted vapour absorption refrigeration system

The general design process involves determining crucial factors such as the component's diameter, length, heat transfer area, and transfer coefficients. When determining a component's performance, the design phase seems to be the most crucial phase before the measurement of experimental data and applications.

Every component must be planned before it is fabricated, and the accuracy and precision of the design determine how well the component will function in real life. The primary goal of the design created for this study was to understand the specifics of each component, as seen in Fig. 1.

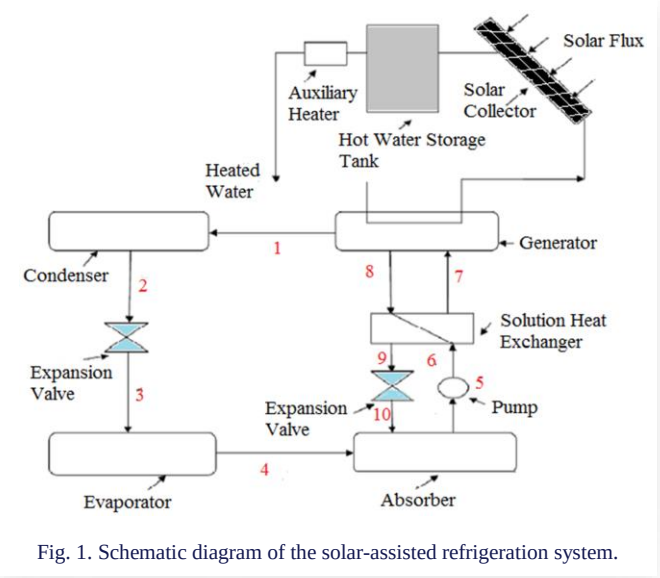

Fig. 1. Schematic diagram of the solar-assisted refrigeration system.

First, the collector collected the solar energy, which was then stored in the storage tank. The generator then boils water vapour using a solution of lithium bromide and water, using the hot water within the storage tank. The condenser cools the water vapour, which then moves to the evaporator, where it evaporates again at low pressure to cool the required area. Once the strong liquid evacuates the generator and flows to the absorber, a heat exchanger warms the weaker solution coming into the generator. The absorber absorbs the water vapour exiting the evaporators into the strong solution. The ventilated tower's cold water mixes and condenses to remove heat. When solar energy is insufficient to heat the water to the temperature required by the generator, an additional energy source supplies the hot water.

2.2. Thermodynamic analysis of the system

To perform the thermodynamic analysis of the system, key parameters such as enthalpy, mass and heat transfer rates are required to determine the system's coefficient of performance (COP). Initially, a set of thermodynamic mathematical models is developed based on mass flow rates and enthalpy, using energy and mass balance equations for each component. To determine the system's COP, operating conditions such as temperatures, pressures and enthalpies are input into the mathematical models. The thermodynamic analysis of the system is based on the following assumptions:

i. Constant flow and stable state,
ii. No friction-related pressure drops,
iii. In the generator, only pure refrigerant boils.

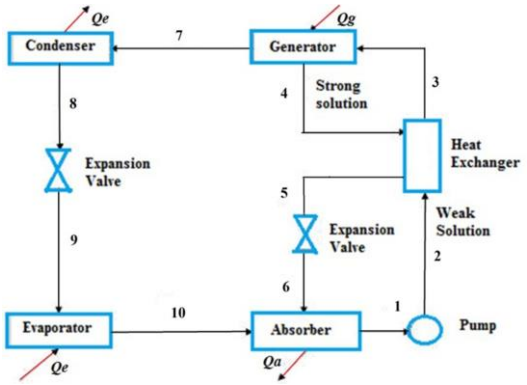

Fig. 2. Block diagram of the absorption vapour refrigeration system.

2.3. Cross-flow heat exchangers with integration of backward splitter plate

We created the geometry using ANSYS Design Modeler and adjusted the mesh to ensure high resolution in flow areas such as the tube surfaces and splitter plate edges. Splitter plate length-to-diameter ratios (L/D) of 0, 0.5, 2 and 3 were taken into consideration in this investigation. Furthermore, the splitter plates have been examined with clockwise rotational inclinations of 15° and 30°, see Table 1. As shown in Fig. 3, the rectangular channel under consideration in this study has dimensions of $L \times W \times H$ of 600 mm, 150 mm and 150 mm, respectively. The cylinder diameter of 25 mm is taken for the study.

Table 1. Range of parameters of the present research work.

Parameter	Parameter details
Length of splitter plate to diameter of tube (L/D) ratio	0.5, 1, 2, 3
Inclination of the splitter plate	+30°, +15°, 0, -30°, -15°
Reynolds number (Re)	2000 – 12 000

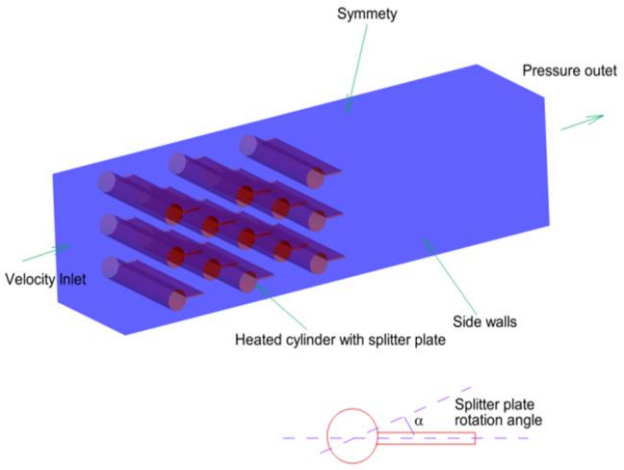

Fig. 3. Computational domain of the present study.

The computational model is depicted in Fig.3. The splitter plate is considered at different inclination angles. The air is considered with a velocity inlet boundary condition and an outlet with a pressure outlet. The cylinder with a splitter is heated with a constant temperature of 350 K. The top and bottom walls are considered symmetry boundary conditions, and the side walls are given adiabatic boundary conditions.

ANSYS Fluent, which depends on the finite volume approach, solves the governing equations by applying the proper boundary conditions. The coupled algorithm resolves the velocity and pressure coupling. The momentum and energy equations are discretised using a second-order upwind approach. While the velocity and continuous residuals must satisfy the convergence requirement of 10^{-6}, the energy residual has to overcome the barrier of 10^{-8}. The mesh that is used for the computational domain, shown in Fig. 4, is created using fluid meshing. The analysis that is currently available uses a tetrahedral mesh with hex core volume meshing.

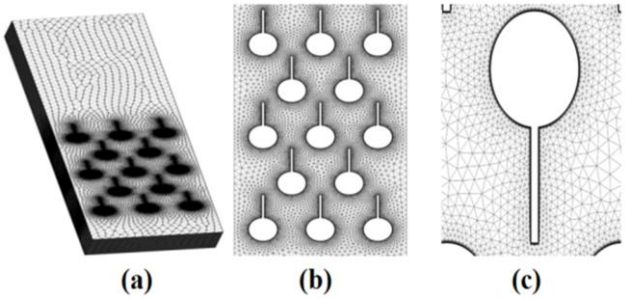

Fig. 4. Mesh at L/D = 2 and α = 15°: (a) computational domain, (b) side view of mesh domain, and (c) enlarged view of meshing of cylinder with splitter plate.

2.3.1. Heat exchanger modelling approach

The heat exchanger was modelled using a 2D steady-state CFD framework to capture flow and temperature distribution within the fluid channels. The governing equations for mass, momentum and energy conservation were solved using the finite volume method. Turbulence effects were captured using the RNG k–ε model, which provides a good balance between accuracy and computational efficiency for internal flows.

2.3.2. Role of the backwards splitter plate

The backward splitter plate was introduced in the design to enhance thermal performance by inducing flow separation and promoting secondary vortices downstream. This geometry forces the fluid to reattach further along the channel, thereby increasing the thermal boundary layer disruption and enhancing convective heat transfer. The position and length of the splitter plate were optimised to avoid excessive pressure drop while maximising thermal enhancement. The backward orientation specifically delays the flow reattachment point and increases residence time in the high-shear region.

2.3.3. Comparison with established correlations

To validate the CFD results, the Nusselt number (Nu) and friction factor (f) obtained from simulations were compared to standard empirical correlations for laminar and turbulent flow in ducts with and without flow disturbances:

- for a smooth channel, the Dittus-Boelter correlation was used for turbulent flow:

$$Nu=0.023Re^{0.8}\,Pr^{0.4},$$

- for laminar flow, the Sieder-Tate correlation was referenced:

$$Nu=1.86(Re\cdot Pr\cdot d\,L)^{1/3}.$$

2.3.4. Computational details, geometry parameters, and mesh independence

The thermal performance and pressure fluctuations in a cross-flow heat exchanger with a grid like circular tube configuration are numerically analysed in this work. To improve heat transfer and control wake dynamics, each tube has a trailing-edge splitter plate. A rectangular duct with 13 circular tubes arranged in a staggered configuration makes up the computing domain (Fig. 5). The industrial applications and design parameters were chosen from the available database for system's heat and mass transfer evaluation. Important characteristics include a 16.4 mm tube diameter, 34.3 mm longitudinal spacing ($SL/D \approx 2.09$), 31.3 mm transverse spacing ($ST/D \approx 1.91$) and 37.7 mm diagonal spacing ($SD/D \approx 2.30$). The ducts 95.4 mm height allow for the accommodation of three rows of tubes across the transverse plane. The overall duct dimensions (190.8 mm in length and width) result in a 2:1 aspect ratio, which ensures controlled flow conditions while maintaining computational efficiency. A rectangular splitter plate that is parallel to the flow direction and has dimensions equal to the tube diameter (16.4 mm) and thickness of 1.75 mm is fastened to the trailing edge of each tube.

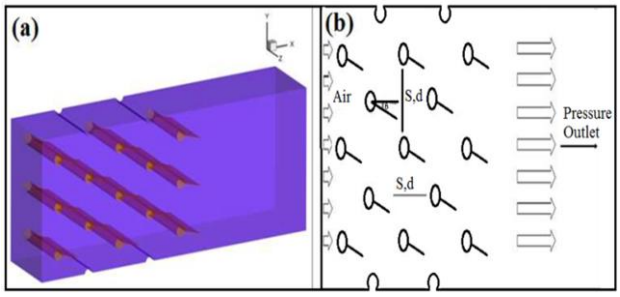

Fig. 5. Schematic view of the computational domain at $L/D = 2$ and $\alpha = 15^{o}$ used in the present study: (a) 3D view, (b) 2D view.

In order to observe wake behaviour and pressure recovery, the computational domain extends 14 tube diameters (229.6 mm) downstream from the first row and two tube diameters (32.8 mm) upstream for appropriate flow development. Four split-tube structures that enforce periodic flow conditions are included in the lateral boundaries to simulate an endless tube bank layout. ANSYS Design Modeler was used to design the geometry, and fine-tuning the meshing ensured good resolution at crucial flow areas like splitter plate edges and tube surfaces. Splitter plate length-to-diameter ratios (L/D) of 0, 0.5, 2 and 3 were taken into consideration in this investigation. Furthermore, the splitter plates have been examined with clockwise rotational inclinations of 15º and 30º. These differences enable a thorough analysis of how splitter plate sizes and orientations affect pressure loss, heat transfer effectiveness and wake dynamics. ANSYS Fluent Meshing was used to perform the meshing process using an unstructured poly-hexcore mesh. This hybrid method includes hexahedral cells in bulk flow regions for computational efficiency, with polyhedral cells close to boundaries for increased accuracy.

The poly-hexcore mesh guarantees numerical stability and improves near-wall resolution. Further refinement would not significantly affect results, since the analysis (Fig. 6) showed a 1.5% difference in pressure drop (ΔP) and a 0.9% difference in Nu between the fine and coarse meshes. Nonetheless, the coarse mesh diverged by as much as 20% from the experimental Nu values, highlighting the need for the fine mesh to strike a balance between computational expense and accuracy.

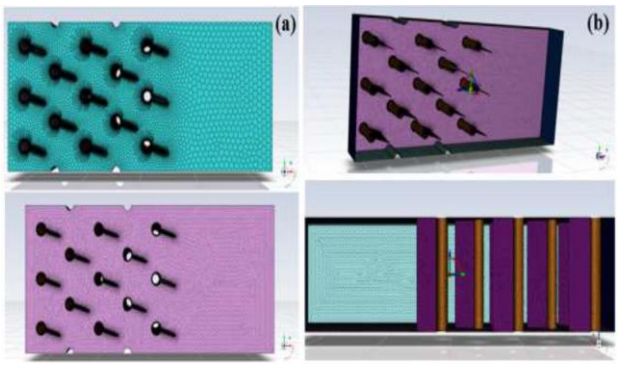

Fig. 6. Mesh used in the present study at $L/D = 2$ and $\alpha = 15^{o}$: (a) coarse mesh, (b) fine mesh at different parts.

2.4. Pressure-temperature-concentration diagram

The primary processes occurring in the system are depicted in the pressure-temperature-concentration ($P–T–\xi$) diagram, shown in Fig. 7, as follows: point 6 displays the state of the solution after the low concentrated solutions are pumped from the absorbers at point 5 on line 5-6-7 to the generator through the heat exchangers. Steps 5-7 do not alter the concentration of the weak solution. On lines 7-8, it is shown that the water vapour in the solution is boiling at a steady pressure. During this process, the weak solution turns into a strong one. The weak solution that travels from the absorber to the generator is employed to exchange heat when the strong solution passes through an absorber, as shown in lines 8-10. The concentration of the strong solution does not change during this process. Water vapour is being absorbed from the evaporator by the absorber's strong solution, as indicated in line 10-5. As indicated in line 6-1-2 the water vapour condenses in the condenser as a result of the cooling water maintaining a steady condensing pressure. Condensed water travels from the condenser to the evaporator via an expansion valve, as shown in lines 2-3. The water in the evaporator is evaporating due to the current low pressure, as lines 3-5 demonstrate. The water also absorbs the heat from the region that needs cooling. The refrigeration cycle is completed when the strong solution in the absorber absorbs the water vapour from the evaporator.

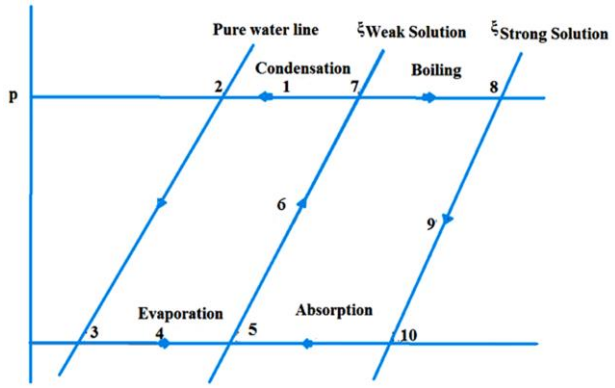

Fig. 7. Diagram of temperature, pressure and concentration (T–P–ζ).

2.5. Thermodynamic analysis and COP evaluation

The validation of the work has been carried out to ensure the accuracy of the results. The current research design primarily involves thermodynamic analysis, including heat and mass transfers for each component, and ultimately the evaluation of the system's COP. In the design process, each of the five components as condenser, evaporator, heat exchanger, generator and absorber was selected based on established process parameters. The system was designed to study how variations in different parameters may affect its actual performance.

The system's COP is its most crucial metric, and it should be as high as possible. Each of the variables that can influence the system's COP should be examined separately. The variables that can affect the system COP in this case are the temperatures of the condensation device, the generator, the absorber and the evaporator. These are the quantities that need to be examined in order to determine how variations in their values may affect the system COP. This type of research is known as the parametric effect. Each of the aforementioned values must be varied separately to examine its impact on COP. To achieve this, the parameter under research is changed while the other parameters remain unchanged. The same procedure is repeated for every parameter. The fundamental equations obtained from the system's thermodynamic analysis can be used for the analysis. The LiBr-water pressure-temperature-concentration-enthalpy chart (Fig. 8) was used to obtain the enthalpy and concentration data. The calculated enthalpy and concentration values corresponding to various temperature values were also directly written in tabular form to avoid repeating the same calculation. Additionally, the approach for determining the system COP for the starting value of a parameter is provided.

The generator operates in the low-temperature range suitable for solar thermal collectors, especially flat plate or evacuated tube types, which typically supply heat in the range of 60–90°C. For our study, we selected generator temperatures around 64°C, aligning with achievable outputs from non-concentrating solar collectors under moderate solar conditions. The evaporator operates at low pressures (~6.1 mmHg) to provide chilled water in the range of 4 – 10°C, which is ideal for space cooling applications in buildings. We selected 4.0°C for analysis to represent conservative cooling requirements. These components reject heat to the environment and typically operate at ambient temperatures or slightly above. We used 30°C for both, representing a warm ambient climate, which is consistent with typical design conditions for solar cooling systems in tropical or subtropical regions. The pressures used (6.1 mmHg and 32 mmHg) correspond to the equilibrium vapour pressures of water at the selected evaporator and condenser temperatures, respectively. These values ensure proper phase changes within each component and are consistent with the thermodynamic properties of the LiBr-water mixture. These operating conditions ensure compatibility with solar thermal energy sources, provide effective cooling, and reflect common configurations in solar cooling applications.

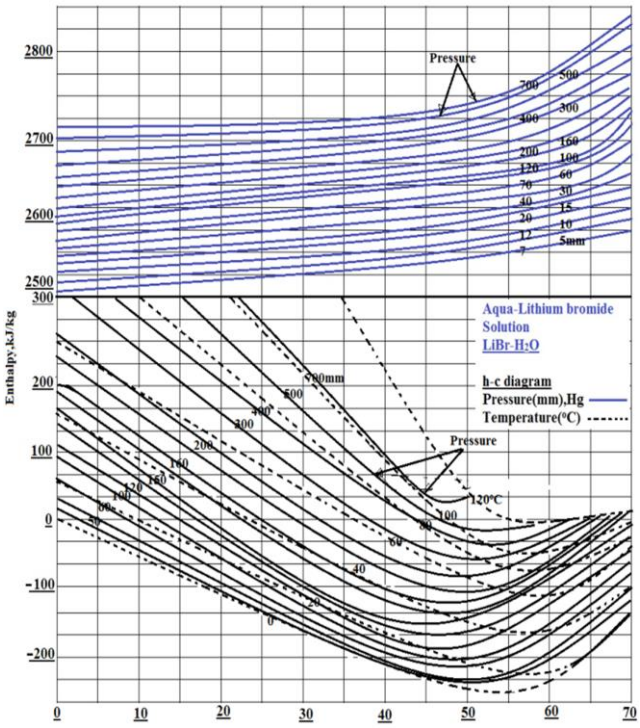

Fig. 8. Lithium bromide (LiBr)-water temperature-pressure-enthalpy-concentration chart.

2.6. Heat and mass balance for each component

Let $\dot{m}$ be the mass circulation rate (measured in kg/s) of the refrigerant, strong solution mass flow rate ($\dot{m}_{ss}$) in kg/s, weak solution mass flow rate($\dot{m}_{ws}$) in kg/s.

2.6.1. Balance for the condenser

The given equations describe the mass flow and heat transfer in a refrigeration system. Specifically, the mass flow rate of the refrigerant at points 7 and 8 is equal, denoted as $\dot{m}_7 = \dot{m}_8 = \dot{m}$, which represents the refrigerant's circulation rate through that section of the system. This equality assumes steady-state operation, meaning the amount of refrigerant entering a component is the same as the amount leaving it. The heat transfer rate Q_c at this section is calculated using the product of the refrigerant's mass flow rate and the difference in specific enthalpy between points 7 and 8, expressed by Eq. (1). This equation essentially

quantifies the energy absorbed or released by the refrigerant due to changes in its enthalpy as it flows through the component.

$$Q_c = \dot{m}(h_7 - h_8), \text{ kJ/s.} \quad (1)$$

2.6.2. Balance for the expansion valve

The mass flow rate of the refrigerant at points 8 and 9 is equal, denoted as $\dot{m}_8 = \dot{m}_9 = \dot{m}$, representing the refrigerant's circulation rate through this part of the system. Additionally, the enthalpy remains constant between these points, indicating an isenthalpic process, typically associated with expansion or throttling in the system. This means that while the refrigerant's pressure or volume may change, no heat is added or removed, and its energy content per unit mass remains the same, expressed in kJ/kg:

$$h_8 = h_9 \text{ (isenthalpic), kJ/kg.} \quad (2)$$

2.6.3. Balance for the evaporator

The mass flow rate of the refrigerant at points 9 and 10 is equal, represented as $\dot{m}_9 = \dot{m}_{10} = \dot{m}$, which denotes the refrigerant's circulation rate through this section of the system. The heat transfer rate Q_e is calculated as the product of the mass flow rate and the change in specific enthalpy between points 9 and 10, expressed as in Eq. (3). This equation quantifies the energy absorbed or released by the refrigerant as it flows through the component, reflecting the system's thermal performance

$$Q_e = \dot{m}(h_{10} - h_9), \text{ kJ/s.} \quad (3)$$

2.6.4. Balance for the absorber

The mass balance for the absorber ensures that the total mass entering equals the total mass leaving, expressed as $\dot{m}_{in} = \dot{m}_{out}$. Here, the refrigerant's mass circulation rate ($\dot{m}$) combined with the strong solution mass flow rate ($\dot{m}_{ss}$) equals the weak solution mass flow rate ($\dot{m}_{ws}$). The circulation ratio, defined as $\lambda = \dot{m}_{ss}/\dot{m}$ allows the weak solution flow to be expressed as $\dot{m}_{ws} = (1+\lambda)\cdot(\dot{m})$.

Applying the mass balance for pure water (mass in − mass out + generation/consumption = accumulation) gives:

$$\dot{m} + (1+\xi_{ss})\cdot\dot{m}_{ss} = (1+\xi_{ws})\cdot\dot{m}_{ws}.$$

The circulation ratio is equal to:

$$\lambda = \xi_{ws}/(\xi_{ss} - \xi_{ws}),$$

and the heat absorbed in the absorber is then calculated, accounting for the enthalpy contributions from the refrigerant and solution flows, as:

$$Q_a = \dot{m}h_{10} + \lambda\dot{m}h_6 - (1+\lambda)\,\dot{m}h_1, \text{ kJ/s.} \quad (4)$$

2.6.5. Balance for the pump

The weak solution mass flow at points 1 and 2 is equal $\dot{m}_1 = \dot{m}_2$ = weak solution mass ($\dot{m}_{ws}$). The work done by the pump is calculated as:

$$W_p = (1+\lambda)\dot{m}V_{sol}(p_c - p_e), \text{ kJ/s,}$$

where V_{sol} is the specific volume of the solution, approximately 0.00055 m^3/kg.

2.6.6. Balance for the solution heat exchanger

For the solution heat exchanger, the weak solution flow remains constant between points 2 and 3, $\dot{m}_2 = \dot{m}_3 = \dot{m}_{ws}$, and the strong solution flow is equal between points 4 and 5, $\dot{m}_4 = \dot{m}_5 = \dot{m}_{ss}$, The heat transfer in the exchanger can be expressed either in terms of the weak solution or in terms of the strong solution as:

$$Q_{hx} = (1+\lambda)\dot{m}(h_3 - h_2) = \lambda\dot{m}(h_4 - h_5), \text{ kJ/s.} \quad (5)$$

2.6.7. Balance for the generator

The mass flow at point 3 is the sum of flows at points 4 and 7, expressed as $\dot{m}_3 = \dot{m}_4 + \dot{m}_7$. The heat supplied to the generator is calculated, accounting for the enthalpy contributions from both the refrigerant and solution streams

$$Q_g = \dot{m}h_7 + \lambda\dot{m}h_4 - (1+\lambda)\dot{m}_3, \text{ kJ/s.} \quad (6)$$

2.6.8. Coefficient of performance

The heat that the refrigerant in the refrigeration system's evaporator absorbs is the system's net refrigerating effect. The sum of the generator's heat supply and the pump's effort is the total energy delivered to the system. Consequently, the system's COP is provided by taking up the following assumption:

- Pump work is neglected (the pump consumes very little energy compared to the heat supplied to the generator; this is due to the pump pressurising a liquid solution, which requires less energy than compressing vapour in vapour-compression systems),
- Steady-state operation is assumed,
- Working fluid mass flow is 1 kg/s of refrigerant unless otherwise noted,
- Heat interactions are assumed:

$$Q_g = h_7 - h_6, \qquad Q_c = h_8 - h_7,$$

$$Q_e = h_{10} - h_9, \qquad Q_{abs} = h_6 - h_9.$$

- COP (coefficient of performance) is defined by:

$$\text{COP} = \frac{\text{Heat absorbed in the evaporator}}{\text{Work done by pump + Heat supplied in the generator}},$$

$$\text{COP} = \frac{Q_e}{(W_p + Q_g)}. \quad (7)$$

Neglecting the pump work in Eq. (7) yields:

$$\text{COP} = \frac{Q_e}{Q_g}. \quad (8)$$

2.6.9. Operating temperatures and pressures

A single effect lithium bromide water refrigeration system has optimal operating temperatures and associated with a COP between 0.7 and 0.9, where T_g as the generator temperature ranges between 55°C and 90°C. The temperature range for the condenser is given as between T_c = 24ºC to 46ºC. Working with a sys-

tem where an absorbent material is absorbing a substance or absorbing heat is suggested by the absorber temperature T_a = 16°C to 32°C. The evaporator temperature range is assumed from T_e = 2.5°C to T_e = 10°C.

2.7. General approach to mass and heat balances

For steady-state operation in an absorption refrigeration system, we apply mass balance and heat balance equations for each component. In each component of the system (generator, condenser, absorber and evaporator), the mass flow rates must be consistent. The mass of refrigerant entering each component is equal to the mass leaving it. The energy entering and leaving each component must balance. The heat entering or leaving a component typically involves the latent heat (associated with phase changes) and the sensible heat (due to temperature changes in fluids).

The generator supplies heat to the refrigerant-absorbent mixture to vaporise the refrigerant (T_g = 64°C, J/kg). In the absorber, the refrigerant vapour is absorbed by the absorbent (e.g. water or lithium bromide) at T_a = 20°C. In the evaporator, the refrigerant absorbs heat from the surrounding medium, the latent heat of vaporisation at T_e = 4°C (J/kg). The operating pressures in proportion to the temperatures can be ascertained. For example, the saturation pressure for condensation in the condenser at 300°C, or 0.0425 bar, can be found using steam tables. In addition, 1 bar equals 750.06 mm of Hg. 0.0425 bar = 32 mm of Hg, which is also equal to the generator pressure, because the condenser and generator operate at the same pressure. Steam tables can now be used once more to calculate the saturation pressure for saturated vapours produced in the evaporator at 40°C because both work at the same pressure. This equals 6.1 mm of Hg, or 0.0081 bar. The refrigerating effect (capacity of the system) is Q_e = 1.5 ton = 5.25 kW.

2.8. Calculation of enthalpy at every designated point of the system

The enthalpy of pure water and superheated water vapours at any temperature can be determined from steam tables. Enthalpies of solutions are calculated from the LiBr-water temperature-pressure-concentration-enthalpy (T–P–ξ–h) chart (Fig. 8).

Table 2. Lithium bromide (Li-Br)-water-temperature-pressure-enthalpy-concentration values.

State points	Temperature, °C	Pressure, mm of Hg	Enthalpy h, kJ/kg	Concentration (ξ)
7	64	32	2616.50	–
8	30	32	125.70	–
9	30	6.1	125.70	–
10	4.0	6.1	2508.70	–
1	20	6.1	−180.0	0.48
2	20	32	−180.0	0.48
3	53.85	32	−115.70	0.48
4	64	32	−120.0	0.56
5	20	32	−195.0	0.56
6	20	6.1	−195.0	0.56

3. Results and discussion

3.1. COP analysis

The proposed finned (splitter plate) heat exchanger's COP calculations have been finished and thoroughly presented. Li-Br-water enthalpy-pressure-temperature-concentration values can be seen from Table 2.

3.2. Data governing equations

The total heat transfer rate can be expressed as:

$$Q_a = \dot{m}(T_{a,o} - T_{a,i}), \tag{9}$$

where $\dot{m}$ is the mass flow rate, and $T_{a,o}$ and $T_{a,i}$ (288 K) are the fluid outlet and inlet temperature, respectively.

The air mass flow rate is given by:

$$\dot{m} = \rho V_{mean} HW, \tag{10}$$

where H and W are the height and width of the duct, respectively.

The total pressure drop and friction factor can be found as:

$$\Delta P = P_{a,i} - P_{a,o}, \tag{11a}$$

$$f = \frac{\Delta P}{\left(\frac{L}{D}\right)\left(\frac{\rho V_{mean}^2}{2}\right)}. \tag{11b}$$

3.3. Obtaining COP for each component

3.3.1. Analysis for the evaporator

Using the energy balance, the refrigerating effect of the evaporator is calculated as:

$$Q_e = \text{refrigerating effect} =$$

$$= \dot{m}(h_{10} - h_9) = \dot{m}\times(2508.70-125.70) = 5.25 \text{ kW}.$$

Here, the mass flow rate of the refrigerant is equal to

$$\dot{m} = 5.25/(2508.70 - 125.70) = 2.203\cdot10^{-3} \text{ kg/s}.$$

This calculation establishes the refrigerant flow required to achieve the desired cooling effect in the evaporator.

The circulation ratio can be expressed by the formula:

$$\lambda = \frac{\xi_{ws}}{\xi_{ss} - \xi_{ws}}, \tag{12}$$

where ξ_{ws} is the state point of the working substance (in this case ξ_{ws} =0.48), and ξ_{ss} is another state point (here ξ_{ss} = 0.56). Substituting these values, the circulation ratio is obtained as

$$\lambda = 0.48/(0.56 - 0.48) = 6.$$

Thus, the mass flow rates for the strong and weak substance can be evaluated as follows:

$$\dot{m}_{ss} = \lambda \times \dot{m} = 13.22\cdot10^{-3} \text{ kg}$$

$$\dot{m}_{ws} = (1+\lambda)\dot{m} = (1 + 6)\times2.203\cdot10^{-3} = 15.42\cdot10^{-3} \text{ kg/s}.$$

3.3.2. Analysis of the absorber

The energy balance for the connected absorber is given by:

$$Q_a = \dot{m}h_{10} + \dot{m}_{ss}h_6 - \dot{m}_{ws}h_1\,, \tag{13}$$

where h_{10}, h_6, h_1 are the specific enthalpies at the respective points. Substituting the known values as $\dot{m} = 2.203\times10^{-3}$ kg/s, $\dot{m}_{ss} = 13.22\times10^{-3}$ kg/s, $\dot{m}_{ws} = 15.42\times10^{-3}$ kg/s, $h_{10} = 2508.70$ kJ/kg, $h_6 = -195$ kJ/kg, $h_1 = -180$ kJ/kg into Eq. (13), one has:

$$Q_a = (2.203\cdot10^{-3}\times2508.70) + (13.22\times10^{-3}\times(-195)) +$$
$$-\,(15.42\cdot10^{-3}\times(-180)) = 5.724 \text{ kW}$$

3.3.3. Analysis of the solution heat exchanger

The energy balance for the heat exchanger is given by:

$$\dot{m}_{ws}\times(h_3 - h_2) = \dot{m}_{ss}\times(h_4 - h_5) =$$
$$= 15.42\times(h_3 + 180) = 13.22\times(-120 + 195), \tag{14}$$

from which one can obtain that

$$h_3 = -115.70 \text{ kJ/kg}.$$

3.3.4. Analysis of the generator

In the generator of an absorption system, heat is supplied to separate the refrigerant (usually vapour) from the solution. So we apply a steady-flow energy balance:

$$Q_g = \dot{m}h_7 + \dot{m}_{ss}h_4 - \dot{m}_{ws}h_3, \tag{15}$$

from which one can obtain that

$$Q_g = (2.203\cdot10^{-3}\times2621.32) + (13.22\cdot10^{-3}\times(-120)) +$$
$$-\,(15.42\cdot10^{-3}\times(-115.70)) = 5.906 \text{ kW}.$$

3.3.5. Analysis of the condenser

The energy balance for the condenser is given by:

$$Q_c = \dot{m}(h_7 - h_8), \tag{16}$$

from which one can obtain that

$$Q_c = 2.203\cdot10^{-3} \times (2616.50 - 125.70) = 5.487 \text{ kW}$$

The final formula to calculate COP is as follows:

$$\text{COP} = \text{desired effect/work Input} = \frac{Q_e}{Q_g} \tag{17}$$

$$\text{COP} = 5250 \text{ W}/5960 \text{ W} = 0.881$$

The absorption system for refrigeration is more appealing to investigators due to its ability to produce a cooling effect using low-grade energy; as a result, solar energy naturally has an excellent prospect in competing with traditional vapour compression technologies. The solar cooling system concept is both technically and financially appropriate because of the abundance of solar radiation. In terms of energy savings and environmental considerations, solar-assisted vapour absorption chillers have been proven to be appropriate substitutes for the current conventional systems. Their application is particularly significant in areas with consistently high levels of sun radiation. Solar-powered cooling systems offer a solution to this problem because many locations lack the infrastructure required to produce energy for food preservation or human comfort. A 1.5 ton solar vapour absorption cooling system has been designed and examined in this work. To determine heat and mass transfers for each system component and, ultimately, the system COP, a thermodynamic analysis of the system has been conducted, taking into account the appropriate temperatures and pressures.

During performance evaluation, the system displays a COP of 0.881. The amount of work required to achieve the desired cooling or heating effect in a system is indicated by COP. The system performance is largely determined by the efficiency of its primary components, the solar collector and absorption system. Among these, the solar collector plays a crucial role in energy transfer, as it combines both conduction and convection processes. Other components rely primarily on conduction for energy transfer. The performance of the system's various components is closely tied to temperature variations. COP reaches its peak at 24°C (0.89) and decreases as the condenser temperature increases, dropping to 0.85 at 45°C. As the generator temperature rises from 55°C to 64°C, COP increases, peaking at 0.881, but then gradually decreases to 0.85 at 77.5°C. This suggests an optimal temperature range for maximum COP. A rise in absorber temperature leads to a decline in COP. The maximum COP of 0.885 occurs at 16°C, decreasing to 0.88 at 24°C. In contrast, as the evaporator temperature rises, COP increases, reaching its highest value of 0.888 at 12°C, up from 0.879 at 2°C.

The design process emphasises thermodynamic principles to optimise the performance of each component. The transfer of heat between moving fluids is a vital physical phenomenon, and numerous heat exchanger designs are employed across diverse applications, including process industries, power generation facilities, and heating, ventilation and air conditioning (HVAC) systems. The main objective of a heat exchanger is to facilitate effective heat transfer from one fluid to another, either through direct interaction or via a separating surface. Heat transfer within these systems operates primarily through conduction and convection, while radiation is generally considered negligible due to its relatively minor impact in comparison [39]. Understanding how temperatures in various components affect COP enables targeted improvements for better system efficiency. Future studies could focus on conducting a total cost analysis of the system, exploring ways to optimise material use and reduce costs while improving system performance. There is room for further enhancements in system design to achieve a higher COP, material savings, and a simplified design process. Investigating practical aspects such as manufacturing processes and real-world implementation of the system could be valuable for scaling the technology. Exploring the impact of other parameters, such as environmental factors or system integration challenges, could offer new insights into optimising the system further [40−43].

The detailed validation of the simulation results against available experimental data demonstrates the accuracy and reli-

ability of our model. This validation is presented in Section 3.4, where simulated state points (temperature, pressure, enthalpy and concentration) are compared with corresponding experimental values reported in the literature. The results show good agreement, with maximum deviations within acceptable limits (up to 64°C for temperature, 32 mm of Hg for pressure and 2616.50 kJ/kg for enthalpy), indicating that the model accurately captures the system behaviour. Furthermore, an uncertainty analysis has been conducted for both experimental measurements and simulation results. Instrumentation accuracy was considered for each measured parameter (e.g. ±0.5°C for temperature, ±1 mmHg for pressure, ±0.1% for concentration). Numerical uncertainty due to discretisation, boundary conditions and convergence criteria was evaluated using the grid convergence index (GCI) method. Sensitivity analysis was also performed to identify the impact of key input parameters on model outputs.

3.4. Measurement uncertainties and limitations

3.4.1. Experimental limitations

Measurement uncertainties in temperature (±0.5°C), pressure (±1 mm Hg) and flow rate (±2%) may affect the precision of derived thermodynamic properties, such as enthalpy and concentration. The experiments assume steady-state operation, but transient fluctuations in temperature and flow may occur during actual operation, especially under varying solar input conditions. Despite insulation, minor heat losses from piping and components and heat gains from the environment are difficult to eliminate entirely, potentially leading to deviations between measured and actual energy balances. Some components (e.g. solution heat exchangers and expansion valves) are treated as ideal in data interpretation, which may overlook real inefficiencies such as pressure drops and incomplete heat exchange.

3.4.2. CFD modelling limitations

Boundary conditions (e.g. uniform inlet velocity, constant wall temperature) were idealised for computational simplicity. In reality, these parameters may vary spatially and temporally. Although a mesh independence study was conducted, the solution accuracy still depends on mesh quality, particularly in regions with high gradients (e.g. near walls or splitter plates). Very fine meshes were avoided to limit computational cost. The model neglects effects such as fouling or corrosion of heat exchanger surfaces, non-ideal absorption/desorption kinetics, thermal expansion or mechanical deformation, and these may influence real-world performance, particularly during long-term operation. The standard k–ε realizable turbulence model was used due to its balance of accuracy and efficiency. However, it may not fully capture complex flow behaviours (e.g. recirculation zones behind splitter plates) as accurately as more advanced models like large eddy simulation (LES) or direct numerical simulation (DNS). Thermo-physical properties of the LiBr-water mixture were taken from standard libraries or literature. In practice, these properties are temperature and concentration-dependent and may vary slightly with real compositions.

3.5. Performance evaluation

The effect of splitter plate length (L/D) at α = 15° is depicted in Fig. 9. Raising the L/D ratio improves heat transfer; at Re = 12 000, the Nusselt number is increased by 90% compared to Re = 2000 when L/D = 2. Nevertheless, pressure drop restrictions significantly increase at L/D = 3, suggesting an optimal trade-off in the design. The friction factor value reaches its maximum when L/D = 2, indicating an ideal balance between losses in pressure and enhancement of heat transfer. Further increasing L/D leads to significant drag consequences, which reduce performance in general.

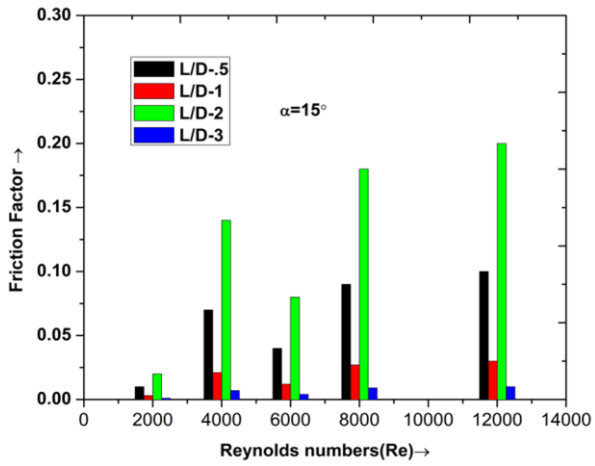

Fig. 9. Effect of splitter plate length on friction factor at a fixed α = 15°.

3.6. Comparative analysis

To evaluate the relative efficiency and novelty of the present LiBr-water absorption system, its key performance metrics, particularly COP and heat transfer rates, are compared with values reported in the literature for similar solar-driven absorption cooling systems.

3.6.1. Coefficient of performance

The current system achieved a calculated COP of 0.881, which is at the higher end of the typical range for single-effect LiBr-water absorption chillers. Table 3 summarises a comparison with selected studies.

Table 3. Comparison of COP with literature.

	COP	Generator temp. (°C)	Evaporator temp. (°C)	System type
Present work	0.881	64	4	Single-effect, solar-assisted
Zhai et al. [40]	0.75	80	7	Single-effect, evacuated tube
Henning [41]	0.70 – 0.80	70 – 95	5 – 10	Single-effect, flat plate
Tawalbeh et al. [42]	0.65	80	10	Single-effect, solar-assisted
Arafia et al. [43]	0.78	85	7	Single-effect, with heat recovery

3.6.2. Heat transfer rates

The heat input and cooling capacity derived from simulation and experimental data are consistent with values reported in prior works:

- evaporator heat transfer rate (Q_e): ~2383 kJ/kg,
- generator heat input (Q_g): ~2811.5 kJ/kg.

These values fall within typical ranges observed in single-effect systems, where Q_g ranges from 2500 – 3200 kJ/kg, and Q_e from 2000 – 2500 kJ/kg, depending on working conditions.

The relatively high COP achieved in this study can be attributed to optimised component design (e.g. use of a backward splitter plate in the heat exchanger). Lower generator temperature requirement (64°C) is compatible with non-concentrating solar collectors. Efficient heat and mass transfer conditions are modelled and controlled in both simulation and experimental setups.

3.6.3. Novelty and practical relevance

Unlike many systems requiring higher generator temperatures (75 – 90°C), the present setup operates effectively at 64°C, making it highly compatible with flat-plate solar collectors. This widens the system's applicability in moderate solar regions, decentralised or low-cost solar installations and retrofitting into existing building cooling infrastructures. The integration of a passively enhanced heat exchanger geometry (via the backward splitter plate) also demonstrates a practical method of improving system performance without additional energy input.

3.7. Enhancement techniques analysis

3.7.1. Passive enhancement techniques

Passive enhancement techniques increase surface area and induce turbulence or secondary flows, significantly improving convective heat transfer. Examples include straight, wavy, pin and annular fins [44]. In solar systems, such geometries have been proven effective for both enhancing performance and managing pressure drop trade-offs. Longitudinal vortex generators (LVGs) are passive devices that create swirling flows, boosting boundary layer disruption and heat transfer in channels or plate heat exchangers [45]. These are increasingly used in compact chiller designs, including asymmetric plate heat exchangers [44]. Inserts like twisted tapes, slotted or wavy tapes and perforated baffles generate turbulence and significantly enhance convective heat transfer. For instance, twisted tape with double-slit inserts can enhance the convective coefficient by 26 – 48%, increasing energy and exergy efficiency by up to ~47% and ~46%, respectively [46]. Such passive methods are simple, robust and widely used. Designed with different channel heights on each side to accommodate varying vapour/liquid properties in LiBr-water systems. These allow compact, efficient heat transfer in absorber and evaporator sections, offering significant space and volume reduction over traditional tube-and-shell designs [44]. Incorporating nanoparticles (e.g. Al_2O_3) into the working fluid can alter thermo-physical properties, raising thermal conductivity and convection performance. Experimental studies demonstrate that such nanofluids maintain similar trending behaviours in COP and component heat loads as base fluids, while offering modest performance improvements [47]. Additives to improve wettability or reduce surface tension have also been applied in absorbers to facilitate film flows and better heat and mass transfer [48−50].

3.7.2. Active enhancement techniques

Mechanical or ultrasonic vibrations can improve film mixing and absorption rates in absorbers. Even though these active techniques have the potential to improve transfer coefficients, reliable results are still scarce and require more research [49]. In latent heat thermal energy storage (LHTES) systems, jet impingement and bubble injection have been explored to accelerate melting/solidification and overcome natural convection limits. These concepts could influence creative chiller component designs even though they are mainly used for storage devices [50].

3.7.3. How our approach builds upon or diverges from these techniques?

This study approaches a backward splitter plate located in the heat exchanger to promote flow separation, create localised vortices and extend the thermal boundary layer. However, like LVGs or twisted tape inserts, the backward splitter plate is a passive, geometry-based enhancement that improves convective heat transfer by disturbing flow patterns and increasing mixing. Unlike conventional forward or twisted inserts, a backward splitter plate reverses flow direction near the trailing edge, optimising separation and reattachment in a controlled manner. It generates localised thermal boundary layer disruption only where needed, potentially achieving enhancement with lower pressure drop than more intrusive inserts. The plate is designed to supplement low-temperature, low-pressure environments typical of solar absorption chillers, making it cost-effective and operationally efficient. In contrast to nanofluid methods or active vibrations, the backward splitter plate requires no additional energy input and avoids the potential complexities of additive-based or active systems. Table 4 summarises several enhancement techniques.

3.8. Future work

To build upon the findings of this study and advance the development of high-performance solar-driven absorption cooling systems, several promising directions for future research are identified. The research indicates that the operational efficiency of a vapour absorption refrigeration system adopting low-cost thermal energy resources might be improved with careful theoretical designing and thermodynamic assessment [51].

3.8.1. Optimisation of system integration

Among promising directions for future research are investigation of the integration of thermal energy storage (TES) systems to buffer intermittent solar input and maintain steady generator operation. Control strategies for real-time load balancing between the collector, TES and chiller should be developed and validated. Multi-objective optimisation techniques (e.g. genetic algorithms or artificial neural networks) could help balance

COP, solar collector area and system cost. Optimisation variables may include generator temperature, flow rates, heat exchanger surface areas and absorber geometry. Hybrid cooling systems combining solar-assisted absorption cooling with photovoltaic-driven vapour compression or desiccant-based dehumidification may be explored, offering improved load flexibility and system redundancy.

Table 4. Enhancement mechanisms and techniques.

Technique	Type	Mechanism	Pros	Cons/Challenges
Fins/extended surfaces	Passive	Increase surface area, induce turbulence	Simple, effective	Possible pressure drop increase
Swirl/vortex generators (e.g., LVG)	Passive	Create swirl secondary flows	Enhanced mixing	More complex geometry
Twisted tapes and Inserts	Passive	Induce swirl, turbulence	High enhancement rates	Increased pressure drop
Asymmetric plate HE	Passive	Tailored channels for vapour/liquid	Compact, efficient	Manufacturing complexity
Nanofluids /additives	Passive	Improve fluid properties	Potential higher conductivity	Stability, cost, potential fouling
Ultrasound /vibration	Active	Enhance film mixing and desorption	Incredible potential	Complexity, limited results
Jet impingement/injection	Active	Enhance convection/ melting	Effective in LHTES	Requires energy input, complexity
Backward splitter plate (this study)	Passive	Promote flow separation and reattachment	Focused enhancement, low drop	Complexity, limited results

3.8.2. Alternative working fluids and mixtures

Investigation of alternative absorbent-refrigerant pairs (e.g. LiCl-H_2O, ammonia-water or ionic liquids) may offer improved performance at lower generator temperatures or reduced material compatibility concerns. Nanofluid-based solutions have shown advantageous effects on thermal conductivity and mass transfer, particularly in the absorber and generator.

3.8.3. Scale-up and manufacturability challenges

Design and construction of larger-scale prototypes that can be integrated into residential or commercial buildings. Then, it can be assessed how well they perform in changing solar and environmental conditions. It is necessary to investigate compact heat exchanger designs (e.g. asymmetric plate, printed circuit or mini-channel heat exchangers) that are suitable for mass production, cost-effective deployment and space-constrained environments. Additionally, it is required to examine the impact of manufacturing tolerances, welding/fabrication processes and long-term material degradation (e.g. corrosion, scaling) on component performance and system reliability.

3.8.4. Control and monitoring strategies

It is necessary to develop intelligent control algorithms based on real-time data acquisition (via IoT sensors) to optimise system operation based on ambient conditions, cooling load and solar availability.

It is also necessary to incorporate diagnostic algorithms to identify early signs of component failure or performance drift, reducing downtime and maintenance costs.

3.8.5. Environmental and economic assessment

Researchers need to conduct a comprehensive life cycle assessment (LCA) to evaluate the environmental impacts of system materials, refrigerants, energy inputs and disposal methods. It is required to perform detailed cost-benefit and payback period analyses under various deployment scenarios (residential, commercial, off-grid) to assess commercial viability. By addressing these areas, future research can bridge the gap between laboratory-scale prototypes and commercially viable, climate-resilient cooling technologies, ultimately contributing to more sustainable and energy-efficient buildings.

4. Conclusions

The conducted analytical study of the solar-operated absorption cooling system's COP provides important information about the effectiveness of the system and its essential parts and reveals that the efficiency of a solar-operated absorption cooling system is largely determined by its primary components, the solar collector and absorption system. Temperature fluctuations significantly affect the performance of these components; the COP reaches its maximum at 24°C and decreases as the condenser temperature increases. Peaks at 0. 881 at 55°C and 0. 881 at 77.5°C indicate the ideal temperature range for the maximum COP.

At a splitter plate angle of $\alpha = 15°$, increasing the length-to-diameter ratio (L/D) enhances heat transfer. At Re = 12 000, the Nusselt number is increased by 90% compared to Re = 2000, when $L/D = 2$. However, pressure drop increases significantly at $L/D = 3$, indicating the need for a design compromise. The friction factor reaches its maximum value at $L/D = 2$, suggesting an ideal balance between pressure losses and heat transfer enhancement. Further increases in L/D have significant drag consequences, which lower performance overall.

Detailed thermodynamic analysis of the system design allows for the optimisation of each component's performance. By understanding how energy and mass interact within the system, this analysis identifies specific areas where improvements can be made, enabling targeted modifications that enhance overall efficiency, reduce energy losses and improve the system's operational effectiveness. Future research directions include cost and material analysis, system improvements, implementation and manufacturing, and exploring additional parameters like environmental factors or system integration challenges. In summary, the analysis confirms the crucial role of temperature regulation in maximising COP. The results highlight a number of promising areas for further research and emphasise the significance of

thermodynamic principles in the design and optimisation of solar-operated absorption cooling systems.

References

[1] Deng, S., Nie, C., Jiang, H., & Ye, W.B. (2019). Evaluation and optimization of thermal performance for a finned double tube latent heat thermal energy storage. *International Journal of Heat and Mass Transfer*, 130, 532–544. doi: 10.1016/j.ijheatmasstransfer.2018.10.126

[2] Zhang, C., Tang, Z., Zhang, Z., Shi, J., Chen, J., & Zhang, M. (2018). Impact of airside fouling on microchannel heat exchangers. *Applied Thermal Engineering*, 128, 42–50. doi: 10.1016/j.applthermaleng.2017.08.163

[3] Tuncer, A.D., Sözen, A., Khanlari, A., Gürbüz, E.Y., & Variyenli, H.İ. (2021). Analysis of thermal performance of an improved shell and helically coiled heat exchanger. *Applied Thermal Engineering*, 184, 116272. doi: 10.1016/j.applthermaleng.2020.116272

[4] Dalkılıç, A.S., Mercan, H., Özçelik, G., & Wongwises, S. (2021). Optimization of the finned double-pipe heat exchanger using nanofluids as working fluids. *Journal of Thermal Analysis and Calorimetry*, 143(2), 859–878. doi: 10.1007/s10973-020-09290-x

[5] Logesh, K., Arunraj, R., Govindan, S., Thangaraj, M., & Yuvashree, G.K. (2020). Numerical investigation on possibility of heat transfer enhancement using reduced weight fin configuration. *International Journal of Ambient Energy*, 41(2), 142–145. doi: 10.1080/01430750.2018.1451382

[6] Fan, Y., Luo, L., & Souyri, B. (2007). Review of solar sorption refrigeration technologies and applications. *Renewable and Sustainable Energy Reviews*, 11, 1758–1775. doi: 10.1016/j.rser.2006.01.007

[7] Jacobsen, A.S. (1977). Solar heating and cooling of mobile homes: Test results. *Proceedings of the Annual Meeting of the American Section of the International Solar Energy Society*, Orlando, FL, USA, June 6–10, pp. 13-15.

[8] Kalogirou, S., Florides, G., Tassou, S. & Wrobel, L. (2001). Design and Construction of a Lithium Bromide Water Absorption Refrigerator. In *Proceedings of CLIMA 2000/Napoli 2001 World Congress.* 15−18 September, Napoli, Italy.

[9] Charters, W.W.S., & Chen, W.D. (1979). Some design aspects of air-cooled solar powered LiBr-H_2O absorption cycle air-conditioning systems. In *Proceedings of the ISES Silver Jubilee Congress* (1, pp. 725–728), May, Atlanta, Georgia, USA.

[10] Mansoori, G.A., & Patel, V. (1979). Thermodynamic basis for the choice of working fluids for solar absorption cooling systems. *Solar Energy*, 22, 483–491. doi: 10.1016/0038-092X(79)90020-3

[11] Zhang, J., Zhu, X., Mondejar, M.E., & Haglind, F. (2019). A review of heat transfer enhancement techniques in plate heat exchangers. *Renewable and Sustainable Energy Reviews*, 101, 305–328. doi: 10.1016/j.rser.2018.11.017

[12] Awad, M., & Muzychka, Y.S. (2011). Models for pressure drop and heat transfer in air-cooled compact wavy fin heat exchangers. *Journal of Enhanced Heat Transfer*, 18(3), 191–213. doi: 10.1615/JEnhHeatTransf.v18.i3.20

[13] Chopra, K., Sahni, V., & Mishra, R.S. (2015). Energy, exergy and sustainability analysis of two-stage vapour compression refrigeration system. *Journal of Thermal Engineering*, 1*(*4), 440–445. doi: 10.18186/jte.95418

[14] Ghamati, M., Askari, N., Moghimi, S.M., Khodadi, S.M., & Taheri, M.H. (2021). Numerical analysis of coupled fluid flow and natural heat transfer on a vertical flat plate. *Journal of Thermal Engineering*, 10*(*1), 1–9. doi: 10.18186/thermal.1428954

[15] Atmaca, I., & Yigit, A. (2003). Simulation of solar-powered absorption cooling system. *Renewable Energy*, 28(8), 1277–1293.

[16] Porumb, R., Porumb, B., & Balan, M. (2017). Numerical investigation on solar absorption chiller with LiBr-H_2O operating conditions and performances. *Energy Procedia*, 112, 108–117. doi: 10.1016/j.egypro.2017.03.1071

[17] Sumathy, K., & Li, Z.F. (1999). Experiments with solar powered adsorption ice maker. *Renewable Energy*, 16, 704–707. doi: 10.1016/S0960-1481(98)00256-0

[18] Pons, M., & Guilleminot, J.J. (1986). Design of an experimental solar powered solid adsorption ice maker. *ASME Journal of Solar Energy Engineering*, 108, 332–337. doi.: 10.1115/1.3268115

[19] Dawoud, B. (2007). A hybrid solar assisted adsorption cooling unit for vaccine storage. *Renewable Energy*, 32, 947–964. doi: 10.1016/j.renene.2006.02.018

[20] Ghali, K., Othmani, M., & Gaddar, N. (2008). Energy consumption and feasibility study of a hybrid desiccant dehumidification air-conditioning system in Beirut. *International Journal of Green Energy*, 5, 360–372. doi: 10.1080/15435070802414280

[21] Abu-Ein, S.Q., Fayyad, S.M., Momani, W., & Al-Bousoul, M. (2009). Performance analysis of solar powered absorption refrigeration system. *Heat and Mass Transfer*, 46(2), 137–145. doi: 10.1007/s00231-009-0538-1

[22] Song, M., Li, N., Shi, F., & Liu, Q. (2024). Performance analysis of a solar single-effect absorption/compression hybrid refrigeration system with integrated absorption energy storage. *Energy Conversion and Management*, 312, 118524. doi: 10.1016/j.enconman.2024.118524

[23] Ayou, D.S., & Coronas, A. (2020). New developments and progress in absorption chillers for solar cooling applications. *Applied Sciences*, 10(12), 4073. doi: 10.3390/app10124073

[24] Sookramoon, K. (2016). Design of a solar tunnel dryer combined heat with a parabolic trough for paddy drying. *Applied Mechanics and Materials*, 851, 239–243. doi: 10.4028/www.scientific.net/AMM.851.239

[25] Banooni, S., & Chitsazan, A. (2016). Effect of solar radiation on the performance of cross flow wet cooling tower in hot climate of Iran. *Heat and Mass Transfer*, 52(11), 2551–2562. doi: 10.1007/s00231-016-1766-9

[26] Ntunde, D.I. (2023). Computational fluid dynamics analysis of a cross flow heat exchanger. *Umudike Journal of Engineering and Technology*, 9(1), 37–45. doi: 10.33922/j.ujet_v9i1_5

[27] Shotlou, A.M., & Pourmahmoud, N. (2023). Frost prediction based on a 3D CFD model of heat and mass transfer in a counter-cross-flow parallel-plate liquid-to-air membrane energy exchanger. *Building Simulation*, 16(11), 2063–2076. doi: 10.1007/s12273-023-1044-y

[28] Shahsavar, A., Yari, O., & Askari, I.B. (2021). The entropy generation analysis of forward and backward laminar water flow in a plate-pin-fin heatsink considering three different splitters. *International Communications in Heat and Mass Transfer*, 120, 105026. doi: 10.1016/j.icheatmasstransfer.2020.105026

[29] Ul-Islam, Z., Ul-Islam, S., & Zhou, C.Y. (2021). Flow control around two side-by-side square cylinders using dual splitter plates. *Journal of the Brazilian Society of Mechanical Sciences and Engineering*, 43(2), 90. doi: 10.1007/s40430-020-02795-4

[30] Chamoli, S., Joshi, A., Rana, S., Bhattacharaya, S., Gupta, A., Ghansela, S., Thianpong, C.,& Eiamsa-ard, S. (2023). Numerical methodology to reduce the drag and control flow around a cam-shaped cylinder integrated with backward splitter plate. *Computation*, 11*(*10), 196. doi: 10.3390/computation11100196

[31] Tu, J., Zhang, Z., Lv, H., Han, Z., Zhou, D., Yang, H., & Fu, S. (2020). Influence of the center cylinder on the flow characteris-

tics of four- and five-cylinder arrays at subcritical Reynolds number. *Ocean Engineering*, 218, 108245. doi: 10.1016/j.oceaneng.2020.108245

[32] Elmekawy, A.M.N., Ibrahim, A.A., Shahin, A.M., Al-Ali, S., & Hassan, G.E. (2021). Performance enhancement for tube bank staggered configuration heat exchanger: CFD study. *Chemical Engineering and Processing: Process Intensification*, 164, 108392. doi: 10.1016/j.cep.2021.108392

[33] Hishikar, P., Gaba, V.K., Dhiman, S.K., & Tiwari, A.K. (2023). Thermal performance of four cylinders in different layouts of spacing ratios under cross-flow at Reynolds number of 35000. *Ocean Engineering*, 281, 114834. doi: 10.1016/j.oceaneng.2023.114834

[34] Duong, C.Q., Luong, T.D., Nguyen, Q.Q., Phung, D.V., & Pham, P.X. (2023). Developing a computational fluid dynamics model for characterizing the heat transfer for a cross-flow plate heat exchanger in a boosted diesel engine. *SAE Technical Paper* 2023-01-5020. doi: 10.4271/2023-01-5020

[35] Hishikar, P., Gaba, V., Dhiman, S., & Tiwari, A. (2025). Heat transfer analysis of nine cylinders arranged inline and staggered at subcritical Reynolds number. *Numerical Heat Transfer, Part A: Applications*, 86(24), 8795–8816. doi: 10.1080/10407782.2024.2363495

[36] Mohankumar, V., & Prakash, K.A. (2024). Numerical investigation of fluid flow and heat transfer characteristics over double backward-facing step with obstacles. *Heat Transfer Engineering*, 45(9), 779–799. doi: 10.1080/01457632.2023.2220474

[37] Rahman, H. (2025). Reduction of drag force for flow around two side-by-side square cylinders through attached upstream splitters. *Journal of the Brazilian Society of Mechanical Sciences and Engineering*, 47(11), 540. doi: 10.1007/s40430-025-05876-4

[38] Illyas, S.M., MuthuManokar, A., & Kabeel, A.E. (2022). Experimental and computational study on effect of vanes on heat transfer and flow structure of swirling impinging jet. *Journal of Applied Fluid Mechanics*, 16(2), 205–221. doi: 10.47176/jafm.16.02.1296

[39] Chauhan, G., Bisht, V.S., Bhandari, P., Singh, S., Shukla, R., Ranakoti, L., & Bist, A.S. (2025). Numerical investigation of heat transfer enhancement in a double pipe heat exchanger using tangential perforated ring turbulators. *Archives of Thermodynamics*, 177–184. doi: 10.24425/ather.2025.154191

[40] Zhai, X.Q., & Wang, R.Z. (2009). A review for absorption and adsorption solar cooling systems in China. *Renewable and Sustainable Energy Reviews*, 13(6–7), 1523–1531. doi: 10.1016/j.rser.2008.09.022

[41] Henning, H.M. (2007). Solar assisted air conditioning of buildings – An overview. *Applied Thermal Engineering*, 27(10), 1734–1749. doi: 10.1016/j.applthermaleng.2006.07.021

[42] Tawalbeh, M., Salameh, T., Albawab, M., Al-Othman, A., El Haj Assad, M., & Alami, A.H. (2020). Parametric study of a single effect lithium bromide–water absorption chiller powered by a renewable heat source. *Journal of Sustainable Development of Energy, Water and Environment Systems*, 8(3), 464–475. doi: 10.13044/j.sdewes.d7.0290

[43] Arafia, M., Soliman, A., & Ossama, A. (2020). A simulation study of n-butane absorption refrigeration system using commercial hydrocarbons as absorbents. *International Journal of Refrigeration*, 112, 110–124. doi: 10.1016/j.ijrefrig.2020.01.004

[44] Ayou, D.S., & Coronas, A. (2020). New developments and progress in absorption chillers for solar cooling applications. *Applied Sciences*, 10(12), 4073. doi: 10.3390/app10124073

[45] He, Y.L., & Zhang, Y. (2012). Advances and outlooks of heat transfer enhancement by longitudinal vortex generators. In: Hewitt, G.F. (Ed.) *Advances in Heat Transfer* (44, pp. 119–185), Elsevier.

[46] Vengadesan, E., & Senthil, R. (2022). Experimental performance enhancement of a flat plate solar collector using straight and twisted flow inserts. *Environmental Science and Pollution Research*, 29(42), 64232–64243. doi: 10.1007/s11356-022-22223-5

[47] Sözen, A., Özbaş, E., Menlik, T., Çakır, M.T., Gürü, M., & Boran, K. (2014). Improving the thermal performance of diffusion absorption refrigeration system with alumina nanofluids: An experimental study. *International Journal of Refrigeration*, 44, 73–80. doi: 10.1016/j.ijrefrig.2014.04.018

[48] Wang, P., Yoon, S., Yu, Y., & Shen, Z. (2019). Experimental study on the active enhancement mechanisms of heat and mass transfer in an absorption chiller (RP-1462). *Science and Technology for the Built Environment*, 25(1), 58–68. doi: 10.1080/23744731.2018.1498668

[49] Raul, R.B., Panda, S.K. (2021). Heat and Mass Transfer-Enhancement Technique Used for Vapour Absorption Refrigeration System. In: Ramgopal, M., Rout, S.K., Sarangi, S.K. (Eds.) *Advances in Air Conditioning and Refrigeration. Lecture Notes in Mechanical Engineering*. Springer, Singapore. doi: 10.1007/978-981-15-6360-7_33

[50] Shank, K., & Tiari, S. (2023). A review on active heat transfer enhancement techniques within latent heat thermal energy storage systems. *Energies*, 16, 4165. doi: 10.3390/en16104165

[51] Ghodeshwar, A., & Sharma, P. (2018). Thermodynamic analysis of lithium bromide–water (LiBr-H_2O) vapor absorption refrigeration system based on solar energy. *International Research Journal of Engineering and Technology*, 5(1), 1365–1371.